J. King Saud Univ., Vol. 18, *Eng. Sci*. (1), pp. 117-137, Riyadh (1426H./2005)

Novel Multi-shell Membrane Reactor for Efficient Dehydrogenation of Ethylbenzene

M. E. E. Abashar and A. A. Al-Rabiah
Chemical Engineering Department, College of Engineering, King Saud University, P.O. Box 800, Riyadh 11421, Saudi Arabia, E-mail address: mabashar@ksu.edu.sa

(Received 26 March, 2005; accepted for publication 13 June, 2005)

Abstract. In this paper, a steady state rigorous mathematical model based on the dusty gas model is implemented to investigate the performance of a novel multi-shell fixed bed membrane reactor for simultaneous production of styrene and cyclohexane. Catalyst patterns for reaction coupling and multi-shell configurations as strong means for shifting the thermodynamic barrier are employed. The simulations show that the complete conversion of ethylbenzene is satisfied only by the combined effect of the membrane and reaction coupling together. The results indicate that effective operating regions with optimal conditions exist. Effective length criteria are used for evaluating the optimal regions. It is shown that these regions are sensitive to changes of catalyst bed composition, feed temperature and pressure. It is also found that the feed temperature has strong influence on the optimal shell ratio. It is also concluded that the multi-shell configuration is superior to the single shell configuration.

Keywords: Ethybenzene, Dusty gas model, Membrane reactor, Multi-shell.

Notation

A_p	external surface area of catalyst pellet, m^2
c_i	concentration of component i in catalyst pellet, $kmol/m^3$
C_i	concentration of component i, $kmol/m^3$
D_{ki}	Knudsen diffusivity of component i, m^2/s
D_i	diffusivity of component i, m^2/s
k_1	reaction 1 rate constant, kmol/kg s kPa
k_2	reaction 2 rate constant, kmol/kg s
K_1	equilibrium constant of reaction 1, kPa
K_B	chemisorption equilibrium constant of benzene, kPa^{-1}
l	axial reactor length, m
L	total reactor length, m
N_i	molar flux of component i, $kmol/m^2$ s

P_i partial pressure of component i, kPa
P_f feed pressure, kPa
Q_o permeability constant, kmol m/m^2 s $Pa^{0.5}$
Q_{H2} hydrogen permeation rate, kmol/ s
r radial distance, m
R'_j rate of reaction j, kmol/kg s
R_1 inner radius of the tube, m
R_2 outer radius of the membrane, m
R_3 inner radius of the shell, m
S membrane area, m^2
T temperature, K
T_f feed temperature, K
u mean velocity, m/s
V_P volume of catalyst pellet, m^3
y_i mole fraction of component i
z catalyst pellet coordinate, m

Greek letters
α_i $= D^t_{ei}\ \psi_1 L/u^t R^2_1$, dimensionless
β $= (1-\psi_1)L/u^t C_{ref}$, m^3.s/kgmol
γ_{ji} stoichiometric coefficient of component i in reaction j, dimensionless
δ membrane thickness, m
ε_j volume fraction of catalyst j, dimensionless
ζ dimensionless axial distance
η_j effectiveness factor of reaction j, dimensionless
θ_i dimensionless concentration of component i
λ_i $=D^s_{ei}\ L/u^s\ \xi^2$, dimensionless
ξ $=R_3-R_2$, m
ρ_j density of catalyst j, kg/m^3
τ characteristic length of the catalyst pellet, m
ψ_1 porosity of the catalytic bed, dimensionless
ψ_2 porosity of the ceramic support, dimensionless
ω dimensionless radial distance

Subscripts
f feed
e effective
ref reference

Superscripts
b bulk
c ceramic support
s shell side
t tube side

Introduction

Styrene is one of the most important monomers as a raw material for synthetic polymers. The recent worldwide production of styrene is estimated at more than 15 million tons per year [1, 2]. Ninety percent of the world production of styrene is manufactured by the catalytic dehydrogenation of ethylbenzene over iron oxide catalysts. The main reaction is endothermic and reversible and severely limited by the thermodynamic equilibrium. The maximum ethylbenzene conversion reported is less than 50% [2]. Moreover, the present commercial processes consume a large amount of energy. Thus, it is highly desirable to search for new processes and to improve the process design [1-7].

In recent years, multi-functional reactors with membranes and catalyst patterns have received increased attention [8-11]. The membranes have numerous advantages: shift of thermodynamic equilibrium, simultaneous reaction and separation of products, enhancement of yield and selectivity, control of reactants distribution and low costs. The catalyst patterns can offer the advantage of reaction coupling, shift of the thermodynamic equilibrium, simultaneous production of more than one product and supply and removal of heat for autothermal operations. The reported results have shown considerable improvement in performance of multi-functional reactors [1, 8-11]. Despite the clear evidence of the multi-functional reactors benefits, still these systems are not well understood and the technology is not commercially utilized. Furthermore, the research community has ignored the subject of multi-shell approach.

The objective of this study is to investigate several ways, which have the potential to improve the performance of membrane reactors for the dehydrogenation of ethylbenzene to styrene. We seek to accomplish this aim by implementing catalyst patterns for reaction coupling of ethylbenzene dehydrogenation with hydrogenation of benzene. This coupling may result in further shift of the thermodynamic equilibrium. Furthermore, the multi-shell approach is also implemented as a strong mean for the shift of thermodynamic equilibrium. For this purpose a rigorous heterogeneous dusty gas model is used which takes into account the combined flux relations. The effects of some key parameters are also investigated.

Reaction Kinetics

The kinetics of the main and coupling reactions are given as follows:

Main reaction

The kinetics of dehydrogenation of ethylbenzene to styrene on iron-promoted catalysts in the absence of side reactions is given by [4, 5]:

$$C_6H_5CH_2CH_3 \; f \quad C_6H_5CHCH_2 + H_2 \tag{1}$$

the rate expression for reaction (1) is given by:

$$R_1' = k_1 \left(P_1 - P_2 P_3 / K_1 \right) \quad , \quad kmol/kg\ s \tag{2}$$

The avoidance of the side reactions in the above kinetics is arrived to through the continuous improvements in kinetics over the years [5].

Coupling reaction

The recent worldwide production of cyclohexane is about 4.7 million tons per year [12]. Cyclohexane is a very important chemical that is used in various industries such as electroplating, solvent extraction and rubber manufacturing. The coupling reaction chosen for this study is hydrogenation of benzene on nickel catalysts to cyclohexane. Other alternative hydrogenation reactions such as reaction of hydrogen with carbon monoxide to form methanol and reaction of hydrogen with nitrogen to form ammonia are possible. The intrinsic kinetics for hydrogenation of benzene on nickel catalysts to cyclohexane is given by:

$$C_6H_6 \quad + \quad 3H_2 \quad \rightarrow \quad C_6H_{12} \tag{3}$$

The corresponding rate expression for the intrinsic kinetics is given by [13]:

$$R_2' = k_2 K_B \frac{P_3 P_4}{\left(1 + K_B P_4\right)\left(P_3 + P_4\right)} \quad , \quad kmol/kg\ s \tag{4}$$

the rate and equilibrium constants are given by:

$$k_1 = 0.01 \times \exp\left(0.851 - \frac{10931.76}{T} \right) \quad , \quad kmol/kg\ s\ kPa \tag{5}$$

$$k_2 = 121.11 \times \exp\left(-\frac{6038.65}{T} \right) \quad , \quad kmol/kg\ s \tag{6}$$

$$K_1 = 100.0 \times \exp\left(-\frac{122725.157 - 126.27T - 2.194 \times 10^{-3} T^2}{RT} \right) \quad , \quad kPa \tag{7}$$

$$K_B = 788.0 \times \exp\left(-\frac{3019.32}{T} \right) \quad , \quad kPa^{-1} \tag{8}$$

where T is the absolute temperature (K).

Hydrogen Permeation Rate

The permeation rate of hydrogen through the high flux composite membrane was assumed to obey the half power pressure law [14]:

$$Q_{H_2} = Q_O \left(\frac{S}{\delta}\right)\left[\sqrt{P^t_{H_2}} - \sqrt{P^s_{H_2}}\right] \quad , \quad \frac{kmol}{s} \tag{9}$$

The permeability constant of hydrogen (Q_o) has been determined experimentally by Gobina *et al.* [15], as follows:

$$Q_o = 1.0061\times10^{-12}\exp\left(-\frac{767.38}{T}\right) \quad , \quad \frac{kmol.m}{m^2.s.Pa^{0.5}} \tag{10}$$

where S is the membrane area (m^2) and is given by πndL. This implies that the number of tubes (n), the membrane tube diameter (d) and length (L) have strong influence on hydrogen permeation.

Model Development

Tube side

A rigorous two-dimensional heterogeneous model based on the dusty gas model is developed. This model simulates the operation under steady state conditions. An isothermal reactor has been assumed since the reactor dimensions used in this study are relatively small that the temperature gradients cannot generate significant temperature difference between the reactor points. Radial convective flow and axial diffusion are neglected and the ideal gas behavior is assumed. For the bulk radial Fickian diffusion is assumed. A schematic diagram of the multi-shell catalytic membrane reactor that contains a well-mixed catalyst pattern is shown in Fig. 1.

We consider here a five-component system (C_8H_{10}, C_8H_8, H_2, C_6H_6, C_6H_{12}) in which hydrogen participates in more than one chemical reaction. A differential molar balance on component i gives:

$$\frac{\partial C^t_i}{\partial l} = \frac{D^t_{e_i}\psi_1}{u^t}\left[\frac{\partial^2 C^t_i}{\partial r^2} + \frac{1}{r}\frac{\partial C^t_i}{\partial r}\right] + \frac{(1-\psi_1)}{u^t}\sum_{j=1}^{n=2}\gamma_{ji}\varepsilon_j\rho_j\eta_j R'_j \quad , \quad 0 < r < R_1 \tag{11}$$

where γ_{ji} is stiochiometric coefficient of component i in the jth reaction (negative for reactants) and ε_j is volume fraction of catalyst j and is given by:

$$\varepsilon_j = \frac{volume\,of\,catalyst\;\;j\,in\;\;a\;\;well\,mixed\;\;catalyst\;\;bed}{volume\,of\;\;a\;\;well\,mixed\;\;catalyst\;\;bed} \tag{12}$$

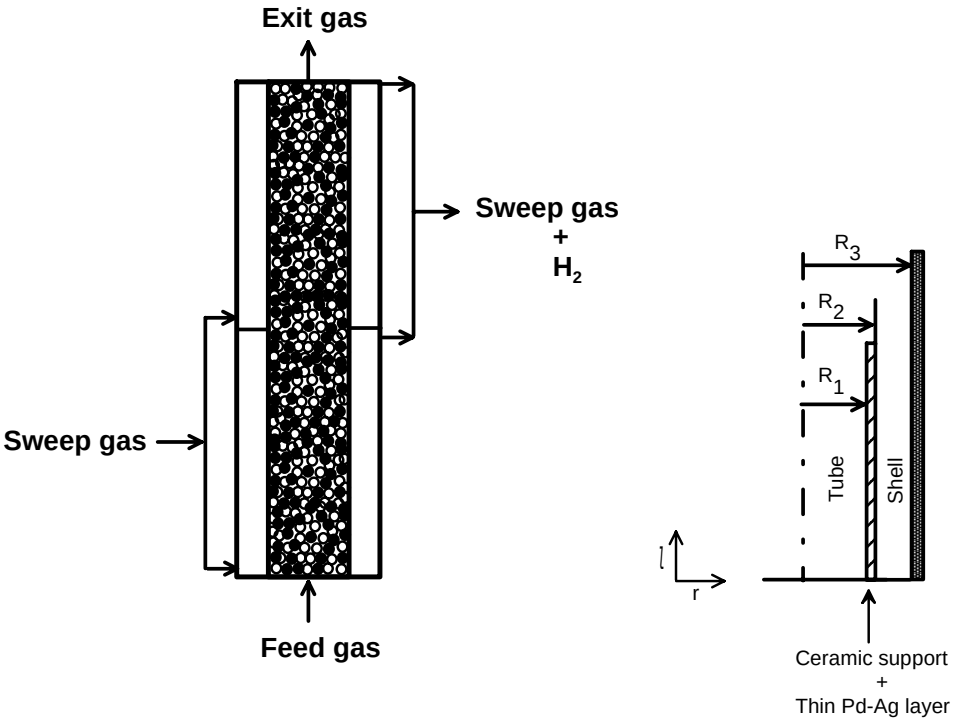

Fig. 1. Schematic representation of the multi-shell catalytic membrane reactor with well-mixed catalysts.

Ceramic support

In the ceramic support, the differential mass balance equation on component i is given by:

$$D^c_{e_i}\psi_2\left[\frac{\partial^2 C^c_i}{\partial r^2}+\frac{1}{r}\frac{\partial C^c_i}{\partial r}\right]=0 \qquad , \quad R_1 < r < R_2 \tag{13}$$

Shell side

The differential mass balance in the shell side gives:

$$\frac{\partial C_i^s}{\partial l} = \frac{D_{e_i}^s}{u^s}\left[\frac{\partial^2 C_i^s}{\partial r^2} + \frac{1}{r}\frac{\partial C_i^s}{\partial r}\right] \qquad , \qquad R_2 < r < R_3 \tag{14}$$

Equations (11), (13) and (14) are coupled together by their boundary conditions as follows:

At the inlet of the reactor:

$$l = 0 \qquad C_i^t = C_{if}^t \qquad , \qquad C_i^s = C_{if}^s \tag{15}$$

At the center of the tube side:

$$r = 0 \quad , \qquad \frac{\partial C_i^t}{\partial r} = 0 \tag{16}$$

At the catalytic layer/ceramic support interface:

$$r = R_1 \quad , \quad C_i^t = C_i^c \quad , \quad D_{e_i}^t \psi_1 \frac{\partial C_i^t}{\partial r} = D_{e_i}^c \psi_2 \frac{\partial C_i^c}{\partial r} \quad , \qquad i = 1-5 \tag{17}$$

At the ceramic support/shell side interface:

$$r = R_2 \quad , \qquad D_{e_i}^c \psi_2 \frac{\partial C_i^c}{\partial r} = 0 \ , \qquad i \neq H_2 \tag{18}$$

for H_2 :

$$\frac{\partial C_{H_2}^c}{\partial r} = \left(\frac{Q_O}{\delta D_{e_{H_2}}^c \psi_2}\right)\left[\sqrt{P_{H_2}^t} \ - \sqrt{P_{H_2}^s}\right] \tag{19}$$

On the wall of the reactor:

$$r = R_3 \quad , \qquad \frac{\partial C_i^s}{\partial r} = 0 \tag{20}$$

Equation (13) can be solved analytically to give:

$$C_i^c = \frac{C_i^t \ln\frac{R_2}{r} + C_i^s \ln\frac{r}{R_1}}{\ln\frac{R_2}{R_1}} \tag{21}$$

Now let us define the following dimensionless quantities:

$$\omega = \frac{r}{R_1} \quad , \quad 0 < r < R_1$$

$$\omega = \frac{r - R_1}{R_2 - R_1} \quad , \quad R_1 < r < R_2$$

$$\omega = \frac{r - R_2}{R_3 - R_2} \quad , \quad R_2 < r < R_3$$

$$\zeta = \frac{l}{L} \quad , \quad \alpha_i = \frac{D_{e_i}^t \psi_1 L}{u^t R_1^2} \quad , \quad \lambda_i = \frac{D_{e_i}^s L}{u^s \xi^2} \quad , \quad \theta_i = \frac{C_i}{C_{ref}}$$

and the following quantities:

$$\beta = \frac{(1-\psi_1)L}{u^t C_{ref}} \quad , \quad \xi = R_3 - R_2 \tag{22}$$

The effective diffusivity coefficient is calculated from [16]:

$$D_{e_i} = \frac{(1-y_i)}{\sum_{\substack{j=1 \\ j\neq i}}^{m=5} (y_i / D_{ij})} \tag{23}$$

With these substitutions, Eqs. (11) and (14) may be written in dimensionless form as follows:

$$\frac{\partial \theta_i^t}{\partial \zeta} = \alpha_i \left[\frac{\partial^2 \theta_i^t}{\partial \omega^2} + \frac{1}{\omega} \frac{\partial \theta_i^t}{\partial \omega} \right] + \beta \sum_{j=1}^{n=2} \gamma_{ji} \varepsilon_j \rho_j \eta_j R_j' \tag{24}$$

$$\frac{\partial \theta_i^s}{\partial \zeta} = \lambda_i \left[\frac{\partial^2 \theta_i^s}{\partial \omega^2} + \frac{1}{\left(\omega + \frac{R_2}{\xi} \right)} \frac{\partial \theta_i^s}{\partial \omega} \right] \tag{25}$$

Catalyst pellet and the dusty gas model

The catalyst pellet is assumed to be at isothermal steady state conditions and having slab geometry with characteristic length τ [17]. The external mass and heat transfer resistances are assumed to be negligible and the concentration profiles are symmetrical about the center of the pellet. The intraparticle mass balance differential equations are expressed as follows:

$$\frac{dN_i}{dz} = \sum_{j=1}^{n=2} \gamma_{ji} \rho_j R_j' \tag{26}$$

By using the rigorous dusty gas model, the total diffusive flux can be written as [18, 19]:

$$-grad\, c_i = \frac{N_i}{D_{K_i}^e} + \sum_{\substack{j=1 \\ i \neq j}}^{m=5} \frac{y_j N_i - y_i N_j}{D_{ij}^e} \tag{27}$$

with the following boundary conditions:

$$\begin{aligned} z = 0 \quad &, \quad N_i = 0 \\ z = \tau \quad &, \quad c_i = c_i^b \end{aligned} \tag{28}$$

The characteristic length τ is given by [17]:

$$\tau = \frac{V_P}{A_P} \tag{29}$$

where V_P and A_p are the volume and external surface area of the catalyst pellet.

The effective diffusivity of any component (D_i^e) can be obtained from equation (27) by dividing its flux by the negative of its concentration gradient:

$$\frac{1}{D_i^e} = \frac{1}{D_{K_i}^e} + \sum_{\substack{j=1 \\ i \neq j}}^{m=5} \frac{y_j - y_i (N_j / N_i)}{D_{ij}^e} \tag{30}$$

The effectiveness for reaction j is given by:

$$\eta_j = \frac{\int_0^{\tau} R'_j \, dz}{\tau \, R'^{b}_j} \tag{31}$$

Numerical Solution

The global orthogonal collocation technique [20] is implemented to change the set of the partial differential equations (Eqs. (24) and (25)) into a set of ordinary equations. Then, the new set of ordinary differential equations are integrated by an IMSL subroutine (DGEAR) based on a Runge-Kutta-Verner fifth and sixth-order method with automatic step size and double precision to ensure accuracy. The catalyst pellet equations resulting from using the dusty gas model are forming a two-point boundary value problem and solved by the global orthogonal collocation technique. Details of the efficient computation algorithm developed for the dusty gas model is given elsewhere [18].

Results and Discussion

The multi-shell membrane reactor is packed with two well-mixed catalysts, which are involved in the reactions. The well-mixed configuration can be made of composite pellets i.e. the two catalysts are co-extruded into composite pellets or two distinct discrete types of pellets that are physically well mixed. In our case, the well-mixed pattern involves loading the reactor with two catalysts after physical well mixed as shown in Fig. 1.

In order to distinguish between the catalysts employed in this investigation, the catalyst used for dehydrogenation of ethylbenzene (the main reaction) is considered to be catalyst 1 and that used for the hydrogenation of benzene (the coupling reaction) is catalyst 2. Two cases are considered in this study. The first case involves single shell and the second case involves two shells. The data used for this simulation study is shown in Table 1.

Single shell membrane reactor

In order to make fair evaluation to the effect of the coupling reaction and the membrane on the performance of the fixed bed reactor, each factor is tested separately and after that the combined effect is examined. For the membrane reactor a single shell is employed. Figure 2 (a) compares the performance of the fixed bed reactor (FBR), the fixed bed reactor with the coupling reaction (FBR+CR), the fixed bed membrane reactor (FBMR) and the fixed bed membrane reactor with the coupling reaction (FBMR+ CR). As it can be seen that the performance of the fixed bed reactor (FBR) is poor and the reaction attains low equilibrium conversion (32.96%). The reaction is severely limited

by thermodynamic equilibrium and only small part of the reactor is utilized. To test the effect of implementing the coupling reaction on the performance of the fixed bed reactor, a small amount of catalyst 2 is added to catalyst 1 (ε_1 =0.90, ε_2 =0.10) and the mixture is physically well mixed. It is clear that considerable enhancement in ethylbenzene conversion (87.15%) is achieved by the coupling reaction. It is also shown that the fixed bed membrane reactor (FBMR) achieves substantial increase in ethylbenzene conversion (85.89%). The presented results show that the trend in the conversion profiles for these two effects are completely different. It is interesting to note that both effects alone are not sufficient to drive the thermodynamic equilibrium to complete the conversion of ethylbenzene. The combined effect of these factors is shown by the performance of the integrated membrane reactor with coupling reaction (FBMR+ CR). It appears that the complete conversion of ethylbenzene is achieved by this configuration. The corresponding partial pressure of hydrogen along the length of the reactor for all cases is shown in Fig. 2 (b). As it can be seen that the partial pressure passes through a maximum when the coupling reaction and membrane are involved. The occurrence of the maximum could be due to the balance of simultaneous formation, consumption and permeation of hydrogen. The mole fractions of all components in the radial position at four collocation points for the integrated membrane reactor with coupling reaction (FBMR+ CR) are shown in Table 2. It is clear that the profiles are flat in the radial direction. In the analyses that follow the membrane reactor with coupling reaction (FBMR+ CR) is considered.

Table 1. Data for the simulation

Reactor length	1.0 m
Reactor diameter	2.5×10^{-2} m
Membrane thickness	6.0 μm
Catalyst pellet diameter	$4.7\ 5\times 10^{-3}$ m
Porosity of catalyst bed	0.5
Catalyst 1 bulk density	1400 kg/m^3
Catalyst 2 bulk density	1200 kg/m^3
Pressure of sweep gas	101.325 kPa
Feed flowrate (STP)	24.0×10^{-6} m^3/s
Sweep gas flowrate (STP)	5.0×10^{-6} m^3/s
Feed composition	mol%
Ethylbenzene	50.0
Benzene	43.0
Hydrogen	07.0

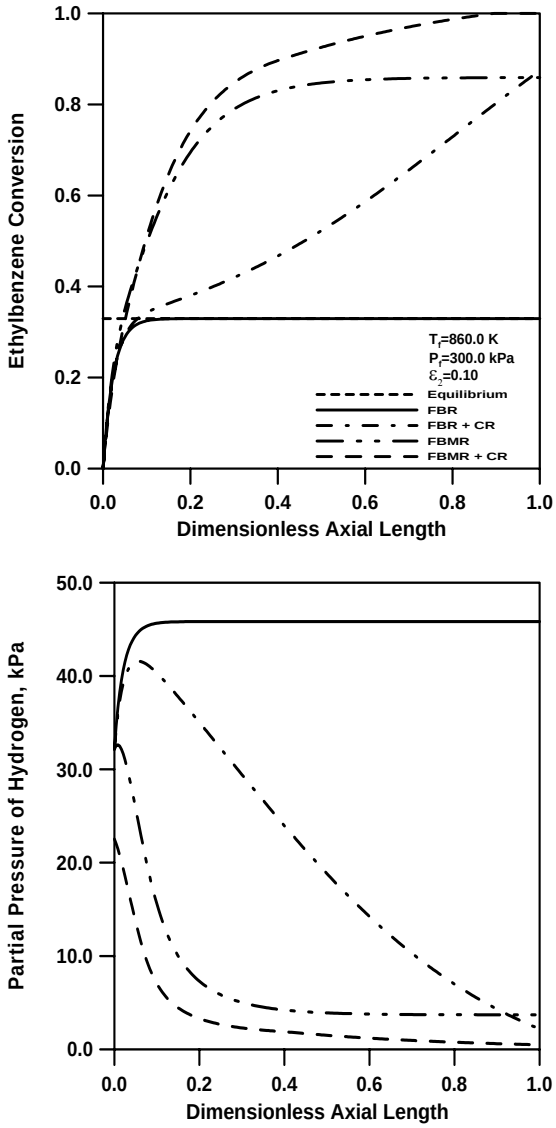

Fig. 2. Comparison of the fixed bed reactor (FBR), fixed bed reactor with the coupling reaction (FBR+CR), fixed bed membrane reactor (FBMR) and fixed bed membrane reactor with coupling reaction (FBMR+CR): (a) ethylbenzene conversion; (b) partial pressure of hydrogen.

Table 2. Axial and radial profiles of all components in the membrane reactor with coupling reaction (FBMR+ CR)

		Radial concentration profiles of components (mol fraction)				
		Collocation point	**1**	**2**	**3**	**4**
Axial position	**Components**	**Radial position**	**0.29760**	**0.63989**	**0.88750**	**1.00000**
0.0	C_8H_{10}		0.50000	0.50000	0.50000	0.50000
	C_8H_8		0.00000	0.00000	0.00000	0.00000
	H_2		0.07000	0.07000	0.07000	0.07000
	C_6H_6		0.43000	0.43000	0.43000	0.43000
	C_6H_{12}		0.00000	0.00000	0.00000	0.00000
0.4	C_8H_{10}		0.05070	0.05070	0.05070	0.05070
	C_8H_8		0.45634	0.45634	0.45634	0.45634
	H_2		0.05689	0.05689	0.05689	0.05685
	C_6H_6		0.31305	0.31305	0.31305	0.31307
	C_6H_{12}		0.12302	0.12302	0.12302	0.12304
0.8	C_8H_{10}		0.01351	0.01351	0.01351	0.01351
	C_8H_8		0.50719	0.50719	0.50719	0.50719
	H_2		0.03737	0.03737	0.03737	0.03730
	C_6H_6		0.30980	0.30980	0.30980	0.30983
	C_6H_{12}		0.13213	0.13213	0.13213	0.13217
1.0	C_8H_{10}		0.00001	0.00001	0.00001	0.00001
	C_8H_8		0.52919	0.52919	0.52919	0.52919
	H_2		0.01525	0.01525	0.01525	0.01525
	C_6H_6		0.29467	0.29467	0.29467	0.29467
	C_6H_{12}		0.16088	0.16088	0.16088	0.16088

The ethylbenzene conversion profiles at different catalyst bed compositions are shown in Fig. 3 (a). It is clearly shown that the addition of catalyst 2 to the bed has significant impact on improving the performance of the reactor. It seems that the benefits of increasing catalyst 2 in the bed is limited to certain compositions beyond which more increase in catalyst 2 has a negative effect on the reactor performance. This could be due to the fact that the increase of catalyst 2 in the bed is at the expense of catalyst 1. As it has been shown in Fig. 3(a) that there is a wide range of bed composition, which gives ≈100% conversion of ethylbenzene at different reactor lengths and in some cases far from the reactor exit, i.e. at shorter reactor lengths. Therefore, in order to investigate the reactor performance in a unified way, we defined a dimensionless effective axial length (ζ_{eff}) as the length of the reactor that gives 99.85% conversion of ethylbenzene. Figure 3 (b) shows the effective axial length versus the composition of the bed. As the concentration of catalyst 2 (ε_2) increases the effective

length tends to assume an inflection point of a minimum value at ε_2=0.3987. Consequently, this bed composition gives an optimum effective length (ζ_{eff} = 0.4333).

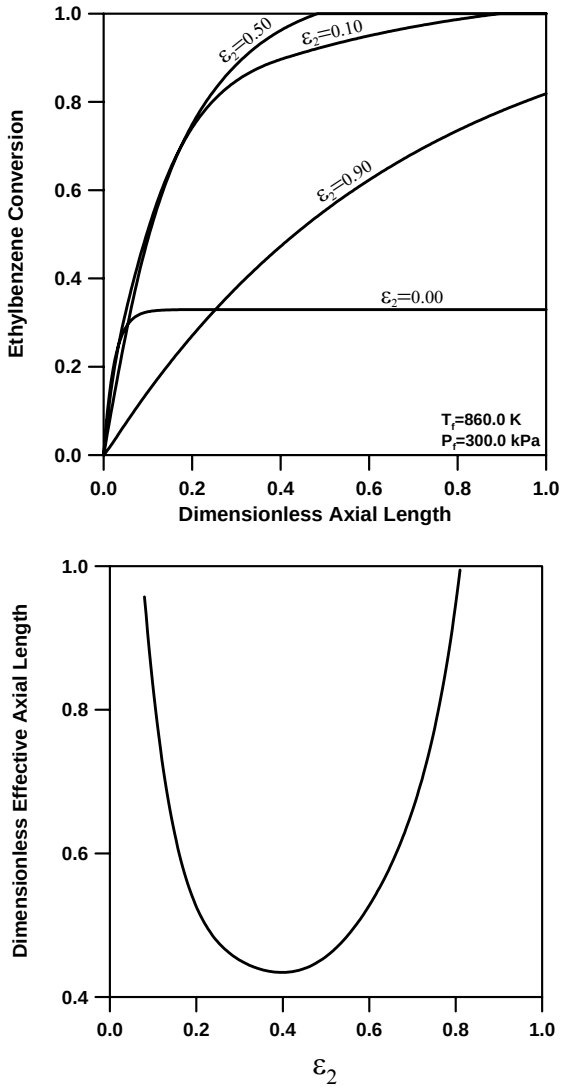

Fig. 3. Fixed bed membrane reactor with coupling reaction (FBMR+CR): (a) ethylbenzene conversion along the reactor for different concentrations of catalyst 2; (b) dimensionless effective axial length as a function of catalyst 2 concentration.

Figure 4 shows the effect of the feed temperature on the effective reactor length. It appears that the feed temperature has a pronounced effect on the effective length, and the optimum effective length is sensitive to the feed temperature changes. However, the optimum bed composition is insensitive to changes of the feed temperature. The complete conversion of ethylbenzene can be achieved at a noticeable decrease in temperature using this kind of reactor. This is very interesting results, since it is known that excessive temperatures have destructive effects on the catalysts and the mechanical stability of the reactors. Moreover, the energy cost is high at elevated temperatures.

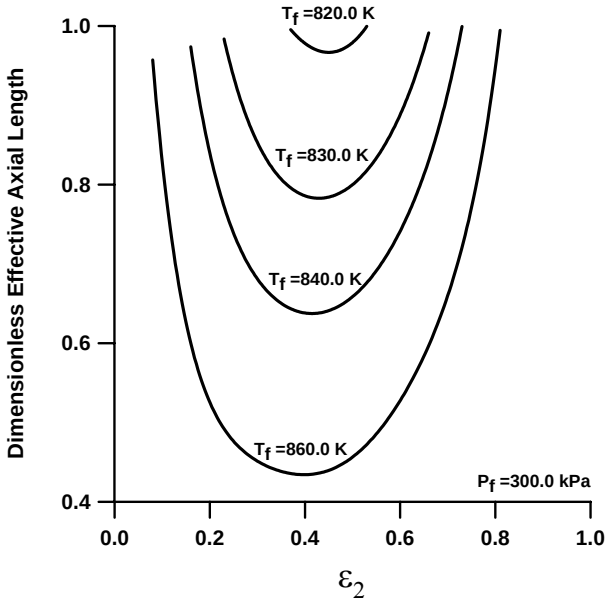

Fig. 4. Effect of catalyst 2 concentration and feed temperature on the dimensionless effective axial length.

Sensitivity analysis for the effect of the feed pressure on the effective axial length is shown in Fig. 5. The increase of the feed pressure favors the hydrogenation reaction of benzene due to the decrease in number of moles (Eq. (3)) and the permeation driving force for hydrogen. There is a noticeable decrease in the effective reactor length when the feed pressure increases. It is interesting to note that the values of the minima decrease and then increase (forming an optimum value) as the feed pressure and the concentration of catalyst 2 increase. The increase of catalyst 2 in the bed, however, is obtained at the expense catalyst 1 which could be the cause of this behavior. It seems that the composition of the bed, feed temperature and pressure should be well controlled.

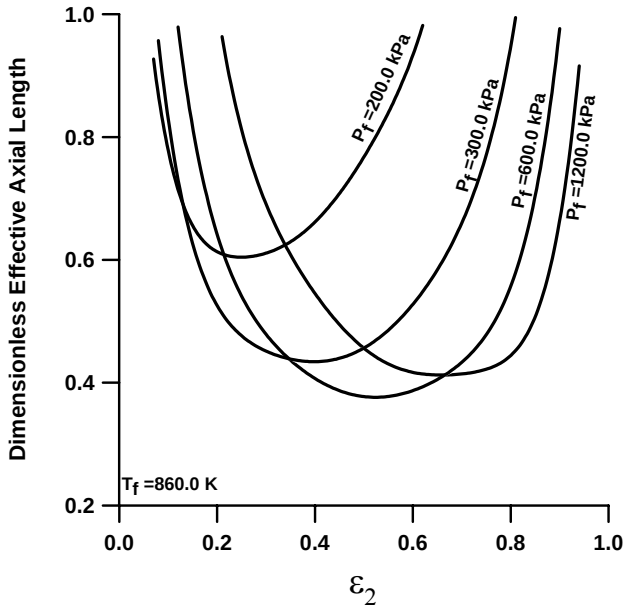

Fig. 5. Effect of catalyst 2 concentration and feed pressure on the dimensionless effective axial length.

Two-shell membrane reactor

In order to achieve further displacement in the thermodynamic equilibrium, the concept of a multi-shell integrated membrane reactor is introuduced. The basic idea behind the shellwise configuration is to enhance the permeation driving force for hydrogen by introducing fresh sweep gas. Two shells are considered in this preliminary investigation. The effect of the shell size on the performance of the fixed bed membrane reactor with coupling reaction is shown in Fig. 6 (a). Three shell ratios are considered (SR_1=1/9, SR_2=1/4, SR_3=2/3). The shell ratio is defined as the volume of shell 1 divided by the volume of shell 2. The shells are numbered from the bottom of the reactor. The results show that for the three shell ratios, the complete conversion of ethylbenzene is satisfied. However, this improvement in ethylbenzene conversion is achieved at different effective reactor lengths. It is clearly shown the superiority of the two-shell configuration over the single shell configuration, i.e. the single shell is the limiting case. The corresponding hydrogen permeation driving force is shown in Fig. 6 (b). As it can be seen that the introduction of fresh sweep gas to the second shell has strong influence in enhancing the permeation driving force for hydrogen. The presented results reveal, in relatively rough form, how the shellwise configuration affects positively the membrane reactor performance.

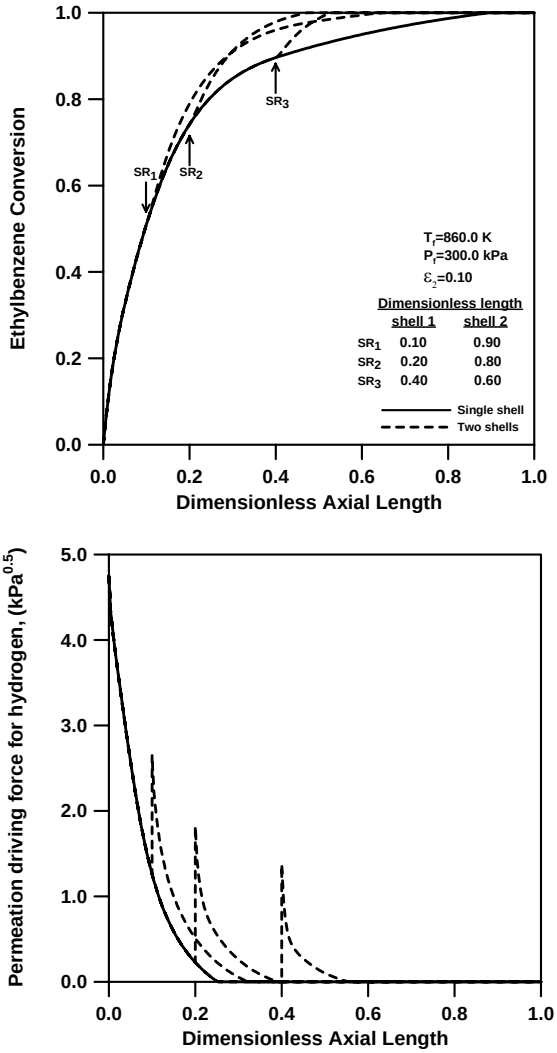

Fig. 6. (a) Ethylbenzene conversion vs. dimensionless axial length for the single-shell and two-shell configurations; (b) corresponding hydrogen permeation driving force for the single shell and two-shell configurations.

Figure 7 shows the effective axial length versus the shell ratio for several bed compositions. It is shown that at a specific bed composition the effective length passes through a minimum with the increase of the shell ratio. The locus of the minima shows that the locations of the minima (at SR≈0.535) are insensitive to the changes in the shell ratios. However, the locations with respect to the effective axial length are sensitive to the bed composition.

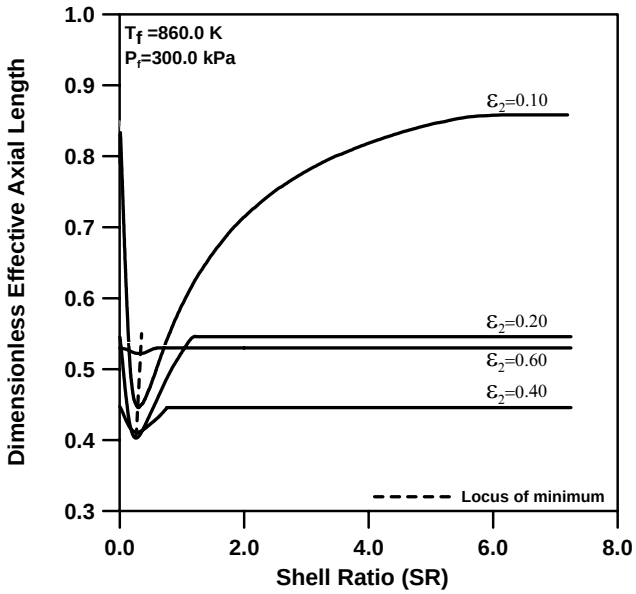

Fig. 7. Effect of shell ratio and catalyst 2 concentration on the dimensionless effective axial length for the two-shell configuration.

The same trend at different feed temperatures is observed. It is found that the minima at feed temperatures (T_f) of 840.0 K and 900.0 K are located at shell ratios (SR) of 0.649 and 0.151 respectively. This result indicates that the optimal shell ratio is strong function of temperature. The influence of the bed composition on the minima is shown in Fig. 8 at different feed temperatures. A computer program is developed to calculate the minima based on Fibonacci search method, which is an efficient region elimination method for a one-dimensional search. As one can see that the curves may assume optimal values of minimum nature with the increase of the composition of catalyst 2 in the bed. The locations of the minima are sensitive to the changes of the bed composition and temperature.

Conclusion

A rigorous mathematical model has been used to investigate the behavior of a multi-shell integrated membrane reactor. Substantial improvement in ethylbenzene conversion over the equilibrium conversion has been achieved by the membrane and coupling reaction. However, the complete conversion of ethylbenzene is satisfied only by the combined effect of the membrane and coupling reaction together. An effective length criterion is used to evaluate the performance of the reactor. The results indicate that effective operating regions with optimal conditions exist. These regions are sensitive to changes of catalyst bed composition, feed temperature and pressure. It is also found that the feed temperature has strong influence on the optimal shell ratio. In the light of

the results presented the multi-shell configuration is shown to be superior to a single shell configuration.

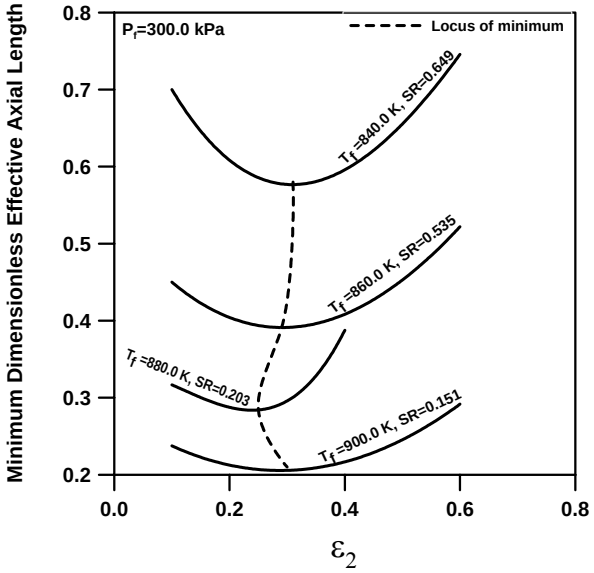

Fig. 8. Effect of catalyst 2 concentration and feed temperature on the minimum dimensionless effective reactor length for the two-shell configuration.

The present study clearly illustrates the potential of a multi-shell integrated membrane reactor in ethylbenzene industry. Further experimental studies are, however, required to assess the reported results. Work along the directions of investigating dual-functionality of catalysts via structured patterns for reaction and energy integration is currently in progress.

References

[1] Abashar, M.E.E. "Integrated Membrane Reactors with Oxygen Input for Dehydrogenation of Ethylbenzene to Styrene." *Proc. of Reg. Sym. on Chem. Eng. and 16th Sym. of Malaysian Chem. Eng.*, Malaysia, October (2002), 1231-1238.

[2] Dittmeyer, R., Höllein, V., Quicker, P., Emig, G., Hausinger, G. and Schmidt, F. "Factors Controlling the Performance of Catalytic Dehydrogenation of Ethylbenzene in Palladium Composite Membrane Reactors." *Chem. Eng. Sci.*, 54 (1999), 1431-1439.

[3] Abdalla, B.K. and Elnashaie, S.S.E.H. "A Membrane Reactor for the Production of Styrene from Ethylbenzene." *J. Membr. Sci.*, 85 (1993), 229-239.

[4] Becker, Y.L., Dixon, A.G., Moser, W.R. and Ma, Y. H. "Modeling of Ethylbenzene Dehydrogenation in a Catalytic Membrane Reactor." *J. Membr Sci*., 77 (1993), 233-244.

[5] Gobina, E., Hou, K. and Hughes, R. "Mathematical Analysis of Ethylbenzene Dehydrogenation: Comparison of Microporous and Dense Membrane Systems." *J. Membr Sci.*, 105 (1995), 163-176.

[6] Moustafa, T.M. and Elnashaie, S.S.E.H. "Simultaneous Production of Styrene and Cyclohexane in an Integrated Membrane Reactor." *J. Membr. Sci.*, 178 (2000), 171-184.

[7] Elnashaie, S.S.E., Abdallah, H.B.K., Elshishini, S.S., Alkhowaiter, S., Noureldeen, M.B. and Alsoudani, T. "On the Link between Intrinsic Catalytic Reactions Kinetics and the Development of Catalytic Processes. Catalytic Dehydrogenation of Ethylbenzene to Styrene." *Catal. Today*, 64 (2001), 151-162.

[8] Cote, A.S., Deglass, W.N. and Ramkrishna, D. "Investigation of Spatially Patterned Catalytic Reactors." *Chem. Eng. Sci.*, 54 (1999), 2627-2635.

[9] Abashar, M.E.E. "Integrated Catalytic Membrane Reactors for Decomposition of Ammonia." *Chem. Eng. and Proc.*, 41 (2002), 403-412.

[10] Abashar, M.E.E., Al-Sughair, Y.S. and Al-Mutaz, I. S. "Investigation of Low Temperature Decomposition of Ammonia Using Spatially Patterned Catalytic Membrane Reactors." *Appl. Catal. A: General*, 236 (2002), 35-53.

[11] Abashar, M.E.E. "Coupling of Ethylbenzene Dehydrogenation and Benzene Hydrogenation Reactions in Fixed Bed Catalytic Reactors." *Chem. Eng. and Proc*., 43 (2004) 1195-1202.

[12] http://www.conocophillips.com/NR/rdonlyres/054ED7CB-21D3-4B20-A1A7-77D D45F6D43B/0/chemicals.pdf.

[13] Marangozis, J.K., Mantzouranis, B. G. and Sophos, A. N. "Intrinsic Kinetics of Hydrogenation of Benzene on Nickel Catalyst Supported on Kieselguhr." *Ind. Eng. Chem. Prod. Res. and Dev*., 18 (1979), 61-73.

[14] Ackerman, F. J. and Koskinas, G. J. "Permeation of Hydrogen and Deuterium Through Palladium-Silver Alloys." *J. Chem. Eng. Data,* 17 (1972), 51-55.

[15] Gobina, E., Hughes, R., Monaghan, D. and Arnell, D. "High Temperature Selective Membranes for Hydrogen Separation." *Dev. Chem. Eng. Min. Proc.,* 2 (1994), 105-114.

[16] Bird, R.B., Stewart, W. E. and Lightfoot, E. N. *Transport Phenomena*. New York: John Wiley, 1960.

[17] Aris, R. "On Shape Factors for Irregular Particles. I. The Steady State Problem, Diffusion and Reaction." *Chem. Eng. Sci*., 6 (1957), 262-265.

[18] Abashar, M.E.E. *Modeling and Simulation of Industrial Natural Gas Steam Reformers and Methanators Using the Dusty Gas Model*. M.Sc. Thesis, UK: University of Salford, 1990.

[19] Mason, E.A. and Malinauskas, A. P. *Gas Transport in Porous Media: The Dusty Gas Model*. Amsterdam: Elsevier, 1983.

[20] Villadsen, J. and Michelsen, M.L. *Solution of Differential Equation Models by Polynomial Approximation.* New Jersey: Prentice-Hall, Inc., 1978.

تركيبة جديدة متعددة الأغلفة لتحسين أداء المفاعلات ذات الأغشية النفاذة لـ ع الهيدروجين من الإيثايلبـ ين

محمد البشير الأمين أبشر وعبدالرحمن بن عبدالعزيز الربيعة

قسم الهندسة الكيميائية، كلية الهندسة، جامعة الملك سعود

ص.ب. ٨٠٠، الرياض ١١٤٢١، المملكة العربية السعودية

(قدِّم للنشر في ٢٠٠٥/٠٣/٢٦م؛ وقبل للنشر في ٢٠٠٥/٠٦/١٣م)

ملخص البحث. استخدم في هذه الورقة نموذج رياضي معقد في حالة الإستقرار ومبني على نموذج الغاز الغباري لدراسة أداء تركيبة جديدة متعددة الأغلفة لتحسين أداء المفاعلات ذات الأغشية النفاذة لإنتاج الإستايرين والسايكلوهكسان معا. استخدمت أنماط من العامل المساعد والأغلفة المتعددة نسبة لكفاءتها العالية في دفع حاجز التحول. أثبتت نتائج المحاكاة أن التحول الكامل للإيثايلبنزين يمكن أن يتحقق فقط بواسطة الغشاء النفاذ والتفاعل المصاحب معا. لوحظ تواجد ظروف مثلي واستخدم الطول المؤثر لوصف تلك الظروف. أثبتت النتائج بأن الظروف المثلي تتأثر بتركيبة العامل المساعد ودرجة حرارة وضغط المغذي، وقد وجد أن درجة حرارة المغذي لها تأثير عميق على نسبة التغليفات المثلي. تمخضت هذه الدراسة بأن التركيبة متعددة الأغلفة تفوق تركيبة الغلاف الواحد.